Applied Catalysis B: Environmental 183 (2016) 53–60

Contents lists available at ScienceDirect

Applied Catalysis B: Environmental

journal homepage: www.elsevier.com/locate/apcatb

Promotion of oxygen reduction and water oxidation at Pt-based electrocatalysts by titanium carbonitride

M. Roca-Ayats [a], E. Herreros [a], G. García [b], M.A. Peña [a], M.V. Martínez-Huerta [a,*]

[a] Institute of Catalysis and Petrochemistry, CSIC, Marie Curie 2, 28049 Madrid, Spain
[b] Faculty of Science, La Laguna University. c/Astrofísico F. Sánchez. 38071, La Laguna, Tenerife, Spain

ARTICLE INFO

Article history:
Received 16 July 2015
Received in revised form 2 October 2015
Accepted 6 October 2015
Available online 20 October 2015

Keywords:
Titanium carbonitride
Oxygen reduction reaction
Oxygen evolution reaction
Bifunctional electrocatalyst
Platinum

ABSTRACT

The oxygen electrode plays a crucial role in performance and lifetime of water electrolyzers and regenerative fuel cells due to its slow electrochemical processes under rigorously oxidizing or reducing environments. Herein, we report the use of titanium carbonitride as an efficient and stable support in acidic media. Pt_3M (M = Ru, Ir, Ta) nanoparticles supported on titanium carbonitride were synthesized by the ethylene glycol method and characterized by transmission electron microscopy, X-ray diffraction and inductively coupled plasma optical emission spectrometry. The electrochemical activity toward oxygen reduction reaction (ORR) and oxygen evolution reaction (OER), as well as the stability of the catalysts, was tested employing a rotating ring-disk electrode. The activity of the three catalysts is similar for the ORR. However, for the OER, Pt_3Ru/TiCN appears to be the best catalyst by far. Pt_3Ru/TiCN was also compared with a commercial RuO_2 catalyst, obtaining a better performance for the supported catalyst even though the low amount of Ru/RuO_2 present in the supported sample. The high activity and stability of the Pt_3Ru/TiCN catalyst for the ORR and OER is due to an interesting promotion effect of the titanium carbonitride support, so that this electrocatalyst has a great potential for the application in unitized regenerative fuel cells.

1. Introduction

It is a truth universally acknowledged that the current energy system needs to be modified in terms of moving toward the implementation of renewable and non-contaminant ways of energy production. For the substitution of the current energy system for a sustainable one based on renewable energies, the implementation of hydrogen as an energy vector seems to be crucial. The cleanest way for obtaining hydrogen is from water electrolysis coupled to a renewable source (photovoltaic solar, wind energy. . .). In this case, the interconversions of water and energy into hydrogen, and hydrogen into electrical energy and water, require the utilization of electrochemical devices [1,2]. An electrolyzer is employed for water splitting, and a fuel cell is required for electrical energy production from hydrogen. As an alternative, unitized regenerative fuel cells (URFCs) are integrated energy storage and conversion systems consisting of a fuel cell and a water electrolyzer in a single unit. As a closed-loop system, it can provide high specific energy density and long-term storage option utilizing renewable energy sources [3,4]. However, the bottleneck of these technologies, in acidic media at low temperature, is the development of catalytic materials active for both electrochemical oxygen reactions, namely the oxygen evolution reaction (OER) and the oxygen reduction reaction (ORR) [5–7]. In ORR, O_2 molecule combines with electrons to form water, whereas OER generates O_2 molecule by taking electrons away from water.

Bifunctional oxygen electrocatalysts are essential in the development of URFCs. They consume oxygen during electricity generation (fuel cell operation), whereas oxygen is evolved during electrolysis mode [5,8]. However, the development of a bifunctional catalyst is not straightforward. Aside from the desired high catalytic activity and good electronic property, bifunctional catalysts should be resistant to anodic corrosion and stable in the acidic medium [9,10]. Moreover, the requirements for a material to catalyze the OER are quite different for those materials that catalyze the ORR [11,12]. For the ORR, the best catalytic materials known are platinum and platinum alloys [7,13–18]. The catalysts are usually made of platinum/platinum alloy nanoparticles supported on carbon materials in order to get a high surface/volume ratio and improve the diffusion of reactants and products. In the other way,

* Corresponding author. Fax: +34 915854760.
E-mail address: mmartinez@icp.csic.es (M.V. Martínez-Huerta).

http://dx.doi.org/10.1016/j.apcatb.2015.10.009
0926-3373/

ruthenium, iridium, ruthenium oxide and iridium oxide and combinations thereof are known to be good electrocatalyst for the OER [7,19–22]. In this case, however, the active phase is used unsupported, as carbon suffers from corrosion at the potentials where the oxygen evolution reaction takes place [7,19,23,24]. In consequence, materials usually employed as bifunctional catalysts for the oxygen electrode of URFCs are a mixture of unsupported platinum and ruthenium, iridium, or its oxides [3,8,25–28].

Few attempts have been done in order to find other catalyst supports resistant enough to be used for the oxygen evolution reaction rather than carbon. It has been reported in literature that for iridium oxide layers deposited onto a titanium substrate, titanium interacts strongly with iridium oxide, increasing the stability of the catalyst. At higher calcination temperatures, with higher presence of titanium oxide, the interaction seems to produce a decrease of the catalyst activity toward the OER due to the formation of titanium-iridium mixed oxides [20,29]. Sui et al. proposed titanium carbide as a suitable support for URFCs oxygen electrocatalysts [30]. They found that compared with the electrocatalysts prepared by chemical reduction and deposition, the novel PtIr/TiC electrocatalyst prepared by plasma reduction displays smaller particles (<5 nm), which are relatively uniform distributed on the surface of the TiC support.

In our previous works, three different titanium-based materials (TiC, TiN and TiCN) were tested as supports for PtIr nanoparticles for the ORR and the OER [31,32]. Titanium nitrides and carbides were chosen because they are extremely resistant materials with high electrical and thermal conductivities. Moreover, they possess an electronic structure near the Fermi level quite similar to that of platinum, which favors the interaction between the support and the platinum nanoparticles [33]. Our previous study established that TiCN was the support with the best balance between activity and stability [32]. To elucidate the promotion effect on different metals by the TiCN support, for both the ORR and the OER, in this work Pt_3M (M: Ir, Ru, Ta) nanoparticles have been incorporated, and the catalytic activity and durability for both electrochemical reactions has been measured by cyclic voltammetry (CV) and linear scan voltammetry (LSV). TiCN supported catalysts were characterized in order to find out correlations between their catalytic behavior and their chemical composition and structure measured by X-ray diffraction (XRD) and transmission electron microscope (TEM).

2. Experimental

2.1. Catalysts synthesis

Three different Pt_3M (M = Ru, Ir, Ta) titanium carbonitride supported catalyst were synthesized. Appropriate amounts of metal precursors ($RuCl_3$ 99.99% from Alfa Aesar, $IrCl_3$ from Johnson Matthey, Tantalum (V) ethoxide 99.98% from Sigma–Aldrich and $PtCl_4$ 99.99% from Alfa Aesar) were employed to obtained catalyst with 20% weight of metals and an atomic ratio 3:1 of Pt:M (M = Ru, Ir, Ta). The three catalysts were labeled as Pt_3Ru/TiCN, Pt_3Ir/TiCN and Pt_3Ta/TiCN. Pt/TiCN catalyst with a nominal Pt loading of 20 wt% was prepared following the same method for a comparison.

The catalysts were synthesized by the polyol method using ethylene glycol (EG) as solvent [34]. Metallic precursors were dispersed in EG and added to a suspension of TiCN ($TiC_{0.7}N_{0.3}$ from Sigma–Aldrich, SA: 22 m^2/g) in the same solvent. After two hours of stirring, the pH was adjusted to 11 and the system was kept at 160 °C under nitrogen flow for three hours. After that, the pH was adjusted to 2 and the catalysts were washed with acetone and water. Finally, a heat treatment was performed under helium flow for one hour at 250 °C.

2.2. Physicochemical characterization

Metal loadings of the catalysts were determined by inductively coupled plasma optical emission spectrometry (ICP-OES) with a with a PerkinElmer Optima 3300 DV spectrometer.

X-ray diffraction profiles of the powder catalysts were obtained on a PANalytical X'Pert Pro X-ray diffractometer with a Cu Kα source. Bragg's angles ranging from 4θ to 90θ were recorded at a scan rate of 0.02θ per second and with an accumulation time of 500 s.

A HRTEM JEOL 2100F operating at an accelerating voltage of 200 kV was used to obtain transmission electronic microscope (TEM) images, which were used to evaluate the morphology and particle size of the catalysts. The average particle diameter of each catalyst was calculated measuring the diameter of at least 300 metallic nanoparticles.

2.3. Electrochemical measurements

All electrochemical measurements were performed in a three-electrode cell controlled by an Autolab PGSTAT302N potentiostat-galvanostat. A reversible hydrogen electrode was used as reference and a carbon row as counter electrode. As working electrode, a rotating ring-disk electrode (RRDE, PINE) composed of a platinum ring and a glassy carbon disk (geometrical area = 0.196 cm^2) with 30 μL of the catalytic ink dried on it was used. The catalytic ink was prepared by sonicating 4 mg of catalyst with 30 μL of Nafion® (5%, Sigma–Aldrich) and 1 mL of water (Milli-Q, Millipore). 0.5 M H_2SO_4 was used as electrolyte. N_2 (99.99%, Air Liquide) was used to deoxygenate the electrolyte and O_2 (99.995%, Air Liquide) for ORR measurements. A commercial RuO_2 catalyst (Alfa Aesar) and Pt/TiCN catalyst were employed as references for the OER and ORR, respectively.

Prior to ORR and OER measurements, catalysts were subjected to an activation process consisting on 50 cycles at 100 mVs^{-1} between 0.05 and 0.8 V in flowing N_2. After that, a blank voltammetry between the same potential limits in N_2 at 20 mVs^{-1} was recorded. The ORR activity was tested with a polarization curve between 1.1 and 0.2 V (negative going scan) with a rate of 2 mVs^{-1} and 1600 rpm in flowing O_2. Prior to ORR polarization curves measurements, the electrode was kept for several minutes at 1.1 V in order to obtain a fully passivated TiCN surface. The initial passivation of the TiCN surface avoids the presence of an oxidation current interference at potentials between 0.9–1.1 V, which could hinder the onset potential determination. ORR measurement was performed while keeping the ring at 1.2 V in order to detect H_2O_2 formation. For the OER measurement, a polarization curve between 0.6 and 1.6 V was recorded at 2 mVs^{-1} and 1600 rpm in flowing N_2. In this case, the ring was kept at 0.4 V (for quantification of the evolved O_2 by ORR) and its signal was differentiated in order to get a better determination of OER onset potential [32]. Between ORR and OER, and after OER, a blank voltammetry was recorded with the same conditions as the initial one in order to get a first idea of the catalysts stability.

For Pt_3Ru/TiCN, an additional stability test was performed. After ORR and OER measurements, the catalyst underwent to a series of experiments trying to simulate the different conditions in which URFC works. This test consists of: (i) 250 cycles between 0.6 and 1.6 V on O_2 saturated electrolyte, (ii) a chronoamperometry at 1.6 V for 10 min and, finally, (iii) a chronoamperometry at 0.05 V and N_2 saturated electrolyte for 20 min.

Blank voltammograms and OER results are normalized by the amount of active metal (Pt + M) on the working electrode, except for the OER comparison between Pt_3Ru/TiCN and commercial RuO_2.

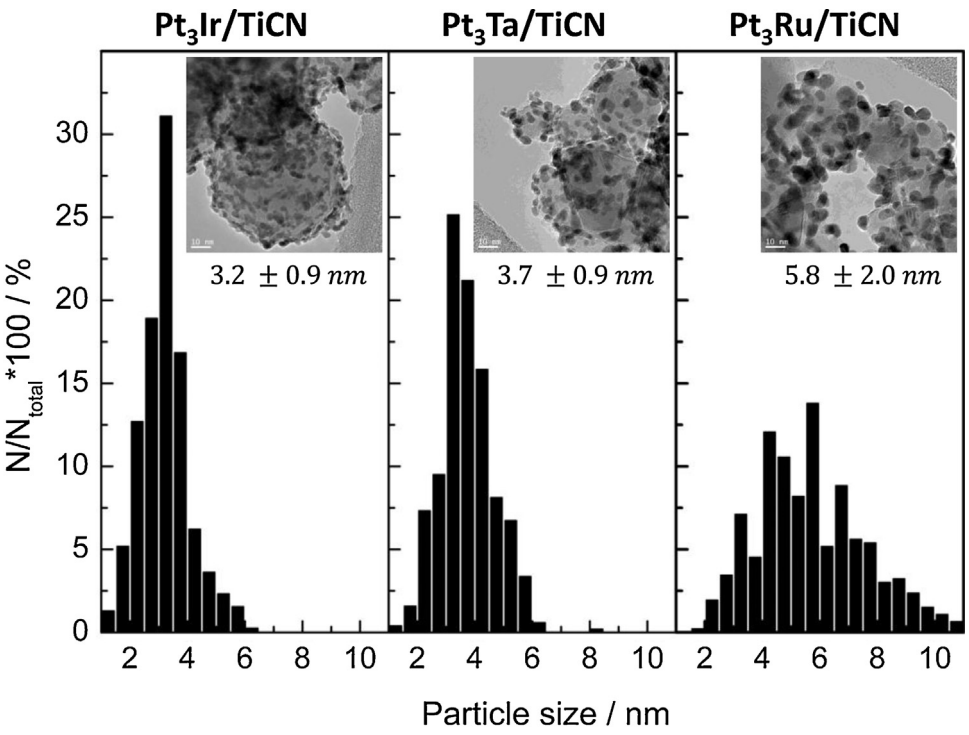

Fig. 1. Transmission electron micrographs and particle size distribution histograms of the catalysts.

In this case, the data is normalized by the mass of Ru in the working electrode. ORR data are normalized by geometric surface area.

3. Results

3.1. Physicochemical characterization

Table 1 summarizes the metal loading and the atomic composition of Pt and M (M = Ru, Ta or Ir) obtained by ICP-OES. Pt_3Ir/TiCN and Pt/TiCN catalysts display similar metal loading and atomic ratio values than the expected from the nominal values. However, a lower metal incorporation was produced for Ru and Ta, and therefore a lower metal M loading and higher atomic ratio of Pt:M than the nominal values were achieved. Nevertheless, similar Pt loading was obtained in Pt_3Ir/TiCN and Pt_3Ru/TiCN catalysts (~13 wt%), but with a lower value for Pt_3Ta/TiCN. Table 1 also includes the average particle sizes and the standard deviation calculated from TEM images. Histograms of particle size distribution and representative TEM images for all catalysts are displayed in Fig. 1. TEM images reveal similar particle size for Pt_3Ir/TiCN and Pt_3Ta/TiCN, whereas Pt_3Ru/TiCN develops larger nanoparticles and a broader particle size distribution. However, similar agglomeration degree of TiCN supported bimetallic nanoparticles is identified for all catalysts.

X-ray diffractograms of the three catalysts are displayed in Fig. 2. All catalysts show the typical highly crystalline cubic pattern of the catalyst support ($TiC_{0.7}N_{0.3}$) (JPCDS 00-042-1489), in addition to the platinum diffraction pattern (JPCDS 00-004-0802). It is noticeable the low intensity of the diffraction patterns of platinum and the second element (Ru, Ir and Ta) in comparison with the high crystalline degree of the catalyst support. The last hinders the metals crystallite size determination by applying the Scherrer equation. Therefore, nanoparticle sizes were not calculated from XRD data and only determined by TEM images. However, some additional information can be extracted from XRD, e.g., Pt_3Ru/TiCN develops a small but visible diffraction pattern associated to the ruthenium oxide tetragonal phase (JPCDS 00-021-1172), whereas Pt_3Ta/TiCN and Pt_3Ir/TiCN do not show patterns related to crystalline oxides.

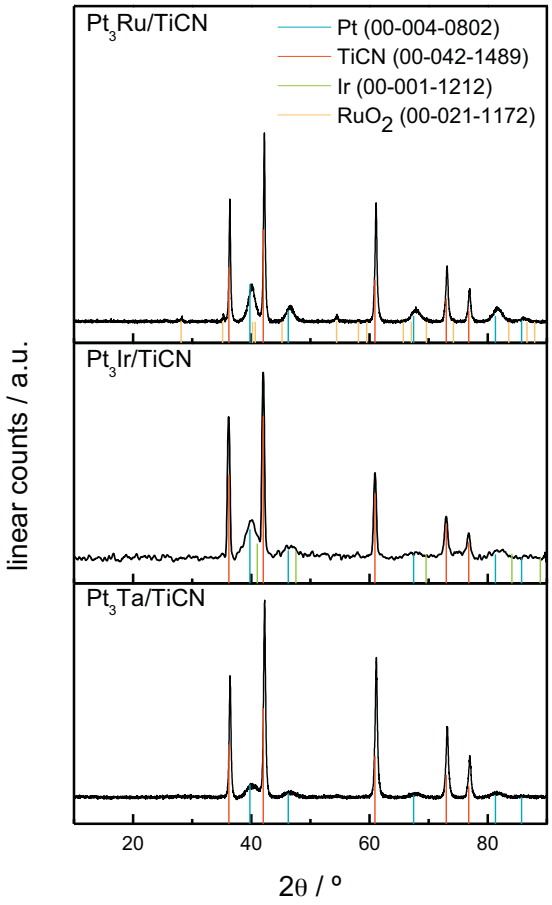

Fig. 2. XRD patterns of Pt_3Ru/TiCN, Pt_3Ir/TiCN and Pt_3Ta/TiCN

Table 1
Physicochemical parameters of the catalysts.

Catalysts	Metal loading Pt + M (wt%)	Atomic ratio Pt:M	Pt loading (wt%)	Average particle size (nm) (TEM)
Pt_3Ir/TiCN	20	2.0	13	3.2 ± 0.9
Pt_3Ru/TiCN	14	4.9	13	5.8 ± 2.0
Pt_3Ta/TiCN	10	4.8	8	3.7 ± 0.9
Pt/TiCN	19	–	19	3.8 ± 1.0

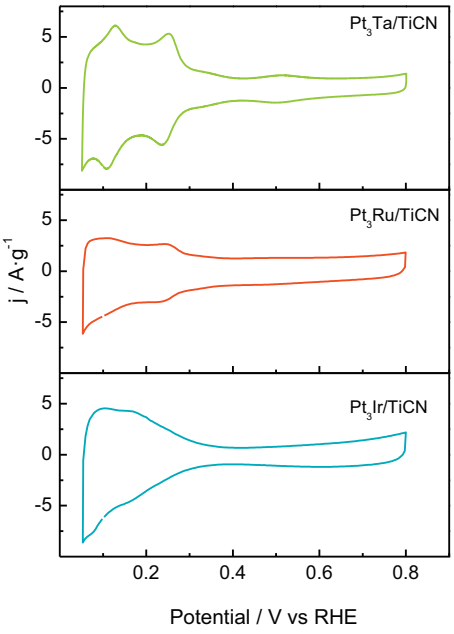

Fig. 3. Blank voltammograms of Pt_3Ru/TiCN, Pt_3Ir/TiCN and Pt_3Ta/TiCN catalysts in 0.5 M H_2SO_4. Scan rate: 20 mV s^{-1}.

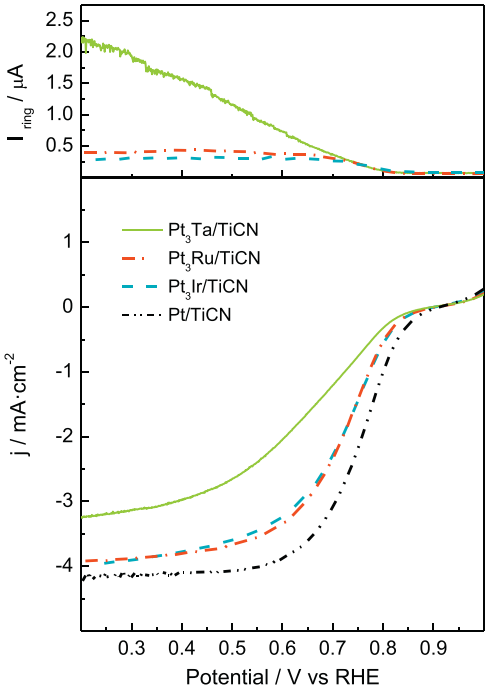

Fig. 4. ORR activities (down) and H_2O_2 current (up) of Pt_3Ru/TiCN, Pt_3Ir/TiCN, Pt_3Ta/TiCN and Pt/TiCN catalysts in 0.5 M H_2SO_4 and 1600 rpm. Scan rate: 2 mV s^{-1}.

However, tantalum oxide is the most stable phase under the current synthesis conditions and, therefore, the presence of amorphous tantalum oxide is expected. Additionally, the presence of amorphous iridium oxide cannot be discarded.

3.2. Electrochemical characterization

Fig. 3 shows the blank voltammograms obtained for the three bimetallic catalysts. Pt_3Ir/TiCN and Pt_3Ru/TiCN develop blanks with a profile far from that of the typical for a nanoparticulated platinum catalyst. The presence of the characteristic hydrogen adsorption/desorption peaks at lower potentials is almost imperceptible, indicating a strong interaction between platinum and the second metal (Ir, Ru). However, for the Pt_3Ta/TiCN catalyst the blank profile is almost identical of that of a monometallic platinum catalyst. The last could indicate that tantalum is not interacting with platinum at all.

3.2.1. Oxygen reduction reaction (ORR)

Fig. 4 shows ORR polarization curves for binary and Pt catalysts recorded in oxygen saturated sulphuric acid solution. Upper panels shows the platinum ring signal (kept at a constant potential of 1.2 V in order to detect H_2O_2 formation) while the lower panel shows the disk signal. For the disk signal, currents are normalized by the geometric area of the electrode (0.196 cm^2) and the deviation of the oxygen solubility due to lower atmospheric pressure is corrected. Similar current profiles are observed for Pt_3Ir/TiCN and Pt_3Ru/TiCN, in which comparable onset potential and diffusional current are obtained. This indicates analogous diffusional properties and catalytic activity toward the ORR. On the other hand, Pt_3Ta/TiCN develops higher onset potential and lower diffusional current, as well as higher H_2O_2 formation, than Pt_3Ir/TiCN and Pt_3Ru/TiCN. This behavior could indicate that there may be a sort of surface impediment, probably the presence of tantalum oxide, hindering the diffusion and readsorption of some intermediates, which decreases H_2O formation and increases H_2O_2 formation, lowering significantly the activity and limiting current for ORR [11,35].

3.2.2. Oxygen evolution reaction (OER)

The water oxidation on Pt_3Ta/TiCN, Pt_3Ir/TiCN and Pt_3Ru/TiCN in acidic medium was studied by the ring-disk technique. The bottom panel of Fig. 5 shows the anodic current delivered by the disk electrode during the anodic sweep potential, whereas the top panel depicts the electric conductance delivered by the ring electrode that is fixed at 0.4 V. Thus, molecular oxygen produced at the disk is further reduced at the ring and consequently the oxygen evolution reaction (OER) can be discerned from by-side reactions.

All catalysts develop an oxidation peak at c.a. 1.1 V during the first weep anodic excursion, which is associated to the surface oxidation of the TiCN support [32,36]. It is noticeable the nonexistence of electric conductance at the ring electrode at this potential, which indicates that any of the species formed during TiCN surface oxidation (CO, CO_2 and probably small amounts of Ti (IV) soluble species) are being reduced at the ring. A similar voltammetric profile was obtained using TiC as support, but not for TiN supported electrocatalysts [32,37]. Indeed, evidence for CO_2 formation at TiCN at potentials higher than 0.9 V in 0.5 M H_2SO_4 was found by in-situ Fourier transform infrared spectroscopy (FTIRS) [36]. In a subse-

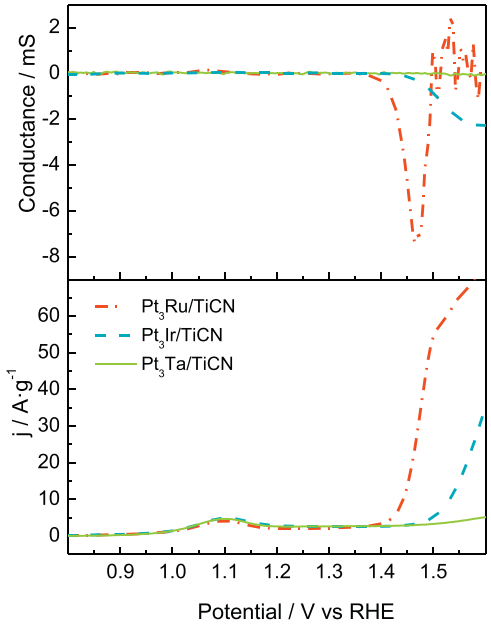

Fig. 5. OER activities of Pt_3Ru/TiCN, Pt_3Ir/TiCN and Pt_3Ta/TiCN catalysts in 0.5 M H_2SO_4 and 1600 rpm. Low panel: disk signal recorded at 2 mV s^{-1}. Top panel: ring's conductance recorded at 0.4 V.

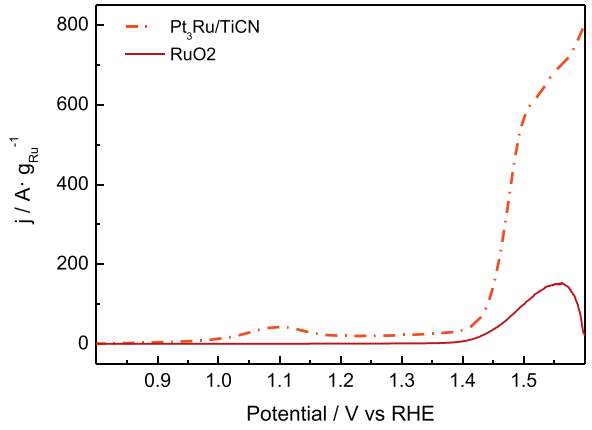

Fig. 6. OER activities of Pt_3Ru/TiCN and commercial RuO_2 recorded at 2 mV s^{-1}, 0.5 M H_2SO_4 and 1600 rpm.

quent OER experiment at TiCN supported catalysts, the anodic peak developed at 1.1 V is not observed. In fact, the anodic peak at 1.1 V is observed again if the working potential is held at low values (e.g., 0.1 V) for several minutes. Therefore, it is expected a surface passivation by Ti oxides at potentials higher than 0.8 V, which avoids further corrosion and maintains high conductivity.

The voltammetric analysis of the TiCN supported catalysts in Fig. 5 show a rise of the anodic faradaic current at higher potentials than 1.3 V for Pt_3Ru/TiCN and Pt_3Ir/TiCN catalysts. Actually, the onset potential for this anodic current increases in the following way: Pt_3Ru/TiCN < Pt_3Ir/TiCN < Pt_3Ta/TiCN. The rise of the ring signal indicates that anodic currents developed at the disk electrode at higher potentials than 1.3 V are related to the water oxidation reaction, i.e., oxygen evolution reaction (OER), since support's oxidation products are not reduced on the ring. Moreover, the measurement of the onset potential is more accurate using the ring signal as by-side reactions are avoided. Using this method, the onset potential values for Pt_3Ru/TiCN and Pt_3Ir/TiCN are 1.37 V and 1.42 V, respectively. It is noticeable the low activity of Pt_3Ta/TiCN toward the OER in this potential range. In fact, a slight modification of the ring signal is achieved, which is related to the low amount of O_2 produced at Pt_3Ta/TiCN. Additionally, the ring signal developed by the Pt_3Ru/TiCN material shows a cathodic electric conductance peak at ca. 1.47 V and at more positive potentials it falls close to zero. Interestingly, the sweep voltammogram develops an anodic hump at the same potential in which the electric conductance ripples. This voltammetric behavior was reported for unsupported and carbon-supported ruthenium nanoparticles, and it was associated to ruthenium oxide species dissolution in acidic media [21]. Therefore, Pt_3Ru/TiCN catalyst develops the highest catalytic activity toward the OER at potentials lower than 1.5 V.

In order to evaluate the effect of the TiCN support toward the OER, unsupported commercial RuO_2 and Pt_3Ru/TiCN catalysts were compared. In this sense, RuO_2 is usually employed as catalyst since it is one of the most active materials toward the OER. Fig. 6 shows the performance of both catalysts during the OER up to 1.6 V. It is important to note that the current is normalized by the amount of ruthenium without taking into account the mass of platinum present in the electrode. Both catalysts reveal similar onset potential for the OER, although the carbonitride-supported material develops higher anodic currents in the whole potential range studied. Indeed, the higher current slope value in the potential range 1.37–1.47 V developed by the Pt_3Ru/TiCN catalyst indicates the faster kinetic of the OER on this material. In the potential range 1.5–1.6 V, some significantly differences are also observed between the supported and unsupported catalysts. For the unsupported catalyst, the current completely decays above 1.55 V. An identical behavior was previously reported for unsupported and carbon supported RuO_2 nanoparticles and was ascribed to extended nanoparticles dissolution [21]. Reier et al. reported that the amount of ruthenium detected by ICP analysis of the electrolyte after the OER on nanoparticulated RuO_2/C corresponds to the complete dissolution of the ruthenium oxide present in the catalyst [21]. In the other side, the decay in activity observed for the TiCN supported catalyst above 1.5 V is not such dramatic. A deviation for the current exponential growth accompanied with decay in ring's current is observed. The later suggests that partial ruthenium oxide dissolution is taking place, but in this case, the current keeps rising, which suggests that not all the active phase is dissolved. As oxygen keeps evolving and neither Pt nor TiCN are active for the OER in this potential range, the activity should be related to the presence of remaining RuO_2

3.2.3. *Catalyst stability*

In order to get a first idea of the catalysts stability, a blank voltammetry was recorded between the ORR and the OER and after the OER tests, with the same conditions as the initial one. It was observed a loose of ESA (electrochemical surface area) after ORR and a partial recovery after the OER in all catalysts.

Additionally, the supported catalyst that performs better, Pt_3Ru/TiCN, was tested with the same stability test performed in our previous work on Pt_3Ir catalysts supported on different titanium-based supports [32]. This test, which aims to reproduce the conditions in which URFC works, consist on subjecting the catalysts to (i) 250 cycles between 0.6 and 1.6 V on O_2 saturated electrolyte, followed by a (ii) 10 min chronoamperometry at 1.6 V on N_2 saturated electrolyte and (iii) 20 min chronoamperometry at 0.05 V on N_2 saturated electrolyte. Finally, the catalysts deactivation was evaluated by recording blank voltammetries between each of the steps of the tests, which were used to obtain the ESA. Fig. 7 shows the ESA (%) drops for Pt_3Ru/TiCN and Pt_3Ir/TiCN catalysts. An ESA drop of 29% was detected, which is a value close to the 30% found for a Pt_3Ir/TiCN catalyst [32].

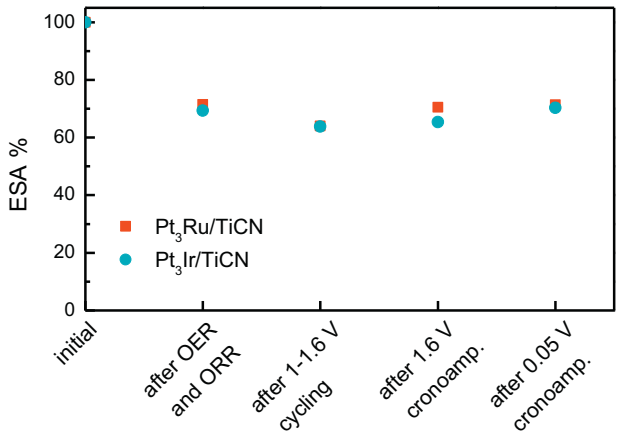

Fig. 7. ESA (%) values of Pt_3Ru/TiCN and Pt_3Ir/TiCN catalysts along stability test.

After the stability test, the catalytic ink used was kept and TEM images were obtained. Fig. 8 shows some of the pictures of Pt_3Ru/TiCN obtained before and after the electrochemical measurements. In the images obtained after stability measurements, it is noticeable the presence of a layer recovering most of the PtRu nanoparticles. This layer was not present on the fresh catalyst. In addition, a slightly increment on particle size and agglomeration degree is observed on the used catalyst.

4. Discussion

The results shown above demonstrate the dependence on the second metal, both on the catalytic activity and morphology, on titanium carbonitride supported bifunctional catalyst for the oxygen electrode.

During the synthesis process, the nature of the second metal affects in a strong way to the metal loading incorporated on the support. The lower incorporation of the second metals seems to concern also the incorporation of platinum. In this way, Pt_3Ta/TiCN is the catalyst with the lowest incorporation of second metal and in this case, the platinum loading is also quite low. It is also important to note that as more noble the second metal is, higher is the metal incorporation. The nobility of the second metal also effects on the atomic ratio Pt:Me, which is higher as less noble is Me, indicating once more that platinum and iridium are easily incorporated. Ruthenium and tantalum are probably not completely reduced during the synthesis process.

Activities reported for the ORR are slightly worse than for pure platinum, both in terms of onset potential and slow raise of current. These results were already expected, since the second added metals show poor activity toward the ORR. The results obtained seem to indicate that the nature of the second metal does not affect the activity of platinum for the ORR in a significantly different way for Pt_3Ru/TiCN and Pt_3Ir/TiCN. However, tantalum seems to affect in a considerably negative way the platinum ORR activity. Onset potential and limiting currents indicate that the presence of tantalum is impeding the reactivity of O_2 and probably the diffusion and readsorption of intermediates, as more H_2O_2 is formed. Another important fact to take into account is the nanoparticles size. It has been reported in literature that the maximum ORR mass activity is achieved for nanoparticles of around 3 nm [38]. However, in this case, Pt_3Ru/TiCN possesses larger nanoparticles (5.8 nm) and its onset potential is not worse than that of Pt_3Ir/TiCN, which possesses an optimum nanoparticles size of 3.2 nm. This could indicate that ruthenium is not affecting the platinum ORR activity in such a negative way as tantalum and iridium do.

For the oxygen evolution reaction results, the onset potentials obtained for the Pt_3Ru/TiCN, RuO_2 and Pt_3Ir/TiCN catalysts are in agreement with those found in literature for unsupported Ir/IrO_2 and RuO_2 nanoparticles[19,39]. It is important to note the considerable lower onset potential for the ruthenium-containing catalyst, which has to be ascribed to the presence of RuO_2 phase observed by XRD. The presence of tantalum seems not to have any effect on the water oxidation, as no significant signal is observed in the ring. The presence of the TiCN support does not hindered the oxygen evolution reaction on these catalysts. Moreover, the catalyst support allows a better active phase dispersion, which results in a higher OER activity even the small amounts of ruthenium and iridium incorporated. This is especially clear on Fig. 6, where Pt_3Ru/TiCN and RuO_2 are compared. In this case, the presence of TiCN support allows a higher utilization of ruthenium oxide phases, as the typ-

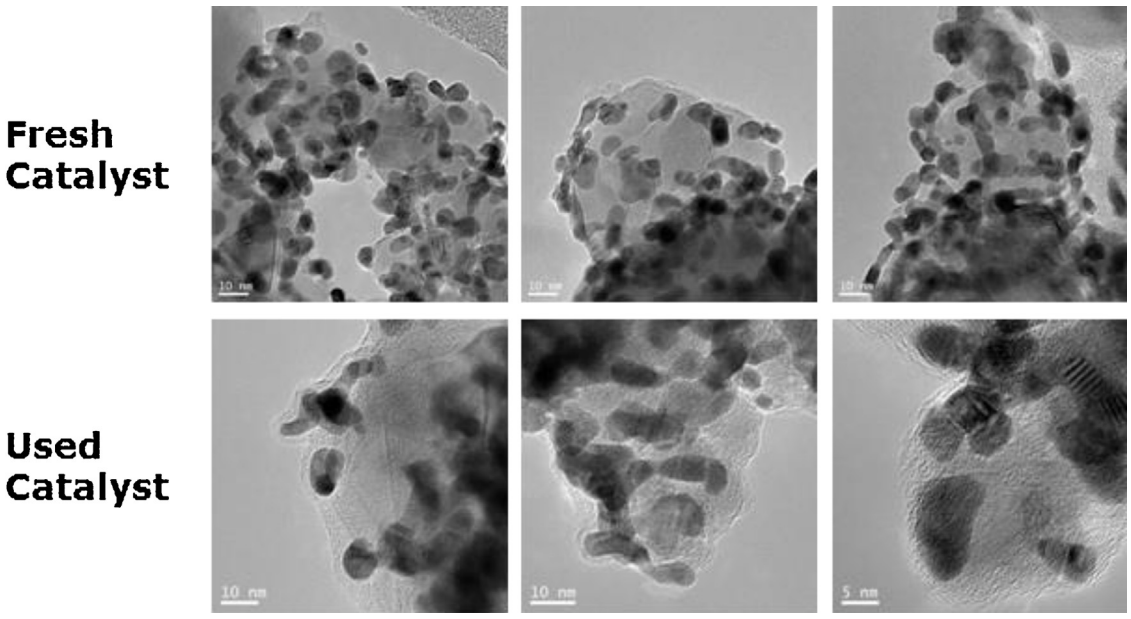

Fig. 8. Transmission electron micrographs of Pt_3Ru/TiCN prior electrochemical measurement and after electrochemical stability test.

ical agglomeration of unsupported nanoparticles is avoided. The better activity of Pt_3Ru/TiCN catalyst in comparison to RuO_2 may not be only due to the better dispersion of the active phase. A previous study by Näslund et al. showed that RuO_2 dopped with TiO_2 is 13% more active than undopped RuO_2 [40]. The dopped coating also appeared to be more stable. TiCN is known to become surface oxidized above 0.8 V indicating that at the potentials where OER takes place, the presence of surface titanium oxides should be considered. This titanium oxide may promote the reaction and play a crucial role on stability of the active phase

Even the better performance of RuO_2 catalysts, IrO_2 is usually employed for this reaction due to the low stability of ruthenium oxide phases in acidic media [19,22,41]. However, in Fig. 6, it is observable that the decay in the supported Pt_3Ru/TiCN is not such dramatic. A similar performance than unsupported RuO_2 has been reported for ruthenium nanoparticles supported on carbon [32]. With the help of the ring current, we were able to determine that for Pt_3Ru/TiCN, the oxygen production decay at 1.6 V is quite lower than for unsupported RuO_2. These results suggest that the TiCN catalytic support not only disperses well the active phase but also contributes on the stabilization of active ruthenium oxide phase. Stability test of Fig. 7 suggests that the stability of Pt_3Ru/TiCN is similar than that of a Pt_3Ir/TiCN catalyst, which could indicate that the presence of the titanium carbonitride or a surface layer of titanium oxide formed at high potential is stabilizing in a similar way the ruthenium and iridium phases, giving rise to an acceptable performance at higher potentials. It is important to remember that it has been reported in literature that the presence of dopping TiO_2 on RuO_2 contributes considerably in the stability of these catalysts [40]. It has been also reported that titanium stabilizes iridium oxide catalysts [20].

In the blank voltammetries recorded after ORR and after OER, a similar behavior on all catalysts was observed. A loss of electrochemical surface area was recorded after ORR, with a partial recovery after OER. The formation of poisoning species during ORR, with its adsorption on the catalysts and its partial removal during OER would explain the ESA decay after ORR and OER recovery.

According to the used-catalysts structure, no significant changes on the nanoparticles size, shape and morphology are observed, only a slightly increase on nanoparticle size. However, the presence of a layer with the same appearance as the support surrounding the nanoparticles was observed by TEM images in the used Pt_3Ru/TiCN catalyst (Fig. 8). This effect was particularly evident in the Ru-based catalyst, while was hardly observed on Ir-based catalyst, and it was not detected on Ta-based catalyst. The partial dissolution of the support at potentials around 1 V in presence of oxygen and the posterior deposition of the species formed during ORR scan toward low potentials would explain the results obtained. The redeposited support would surround the active phase nanoparticles, giving rise to a decrease of ESA. In the OER, however, as the scan starts at lower potentials and goes to positive ones, the dissolution of the support is not followed by redeposition and, in consequence, the ESA is recovered. For catalysts supported on titanium, it was previously observed that the titanium support was corroded by the electrolyte, giving rise to the formation of titanium oxides TiO_x on the catalysts-support interface, which grow until covering the whole interface [7,36,42]. A similar process is proposed to happen in our system, but with the oxide growing or getting deposited around the catalysts nanoparticles. In our case, ruthenium nanoparticles seem to be better stabilized with the surface titanium oxide than other metals, delaying ruthenium dissolution.

5. Conclusions

Three different Pt_3M (M = Ru, Ir or Ta) catalysts supported on titanium carbonitride were evaluated as bifunctional catalysts for the oxygen electrode of unitized regenerative fuel cells. The activity for ORR is similar on iridium and ruthenium based catalysts while for Pt_3Ta/TiCN seems to be impeded. For oxygen evolution reaction, Pt_3Ru/TiCN appears to be the most active one. The stability of this catalyst was found to be similar than that of Pt_3Ir/TiCN, and considerably higher than unsupported RuO_2 nanoparticles. It is proposed that the titanium carbonitride support stabilizes the active phase and delays ruthenium dissolution. A support dissolution/redeposition seems to be occurring.

Acknowledgments

This research was funded by Spanish Ministry of Economy and Competitiveness under projects ENE2014-52158-C2-1R and ENE2014-52158-C2-2R, and partially supported by the European Union Seventh Framework Programme via the EU project DECORE (project 309741) under contract no. FP7-NMP-2012-SMALL-6 for Research and Technological Development. MR acknowledges the FPU-2012 program for financial support.

References

[1] J.O.M. Bockris, Science 176 (1972) 1323.
[2] S.A. Sherif, F. Barbir, T.N. Veziroglu, Sol. Energy 78 (2005) 647–660.
[3] J. Pettersson, B. Ramsey, D. Harrison, J. Power Sources 157 (2006) 28–34.
[4] M. Gabbasa, K. Sopian, A. Fudholi, N. Asim, Int. J. Hydrogen Energy 39 (2014) 17765–17778.
[5] S. Park, Y. Shao, J. Liu, Y. Wang, Energy Environ. Sci. 5 (2012) 9331–9344.
[6] J. Lee, B. Jeong, J.D. Ocon, Curr. Appl. Phys. 13 (2013) 309–321.
[7] I. Katsounaros, S. Cherevko, A.R. Zeradjanin, K.J.J. Mayrhofer, Angew. Chem. Int. Ed. 53 (2014) 102–121.
[8] S. Altmann, T. Kaz, K.A. Friedrich, Electrochim. Acta 56 (2011) 4287–4293.
[9] T. Ioroi, N. Kitazawa, K. Yasuda, Y. Yamamoto, H. Takenaka, J. Electrochem. Soc. 147 (2000) 2018–2022.
[10] Y.N. Zhang, H.M. Zhang, Y.W. Ma, J.B. Cheng, H.X. Zhong, S.D. Song, H.P. Ma, J. Power Sources 195 (2010) 142–145.
[11] L. Jörissen, J. Power Sources 155 (2006) 23–32.
[12] F. Calle-Vallejo, M.T.M. Koper, Electrochim. Acta 84 (2012) 3–11.
[13] H.A. Gasteiger, S.S. Kocha, B. Sompalli, F.T. Wagner, Appl. Catal. B: Environ. 56 (2005) 9–35.
[14] N. Alonso-Vante, Chemphyschem 11 (2010) 2732–2744.
[15] R. Subbaraman, D. Strmcnik, A.P. Paulikas, V.R. Stamenkovic, N.M. Markovic, Chemphyschem 11 (2010) 2825–2833.
[16] J. Herron, J. Jiao, K. Hahn, G. Peng, R. Adzic, M. Mavrikakis, Electrocatalysis 3 (2012) 192–202.
[17] A. Rabis, P. Rodriguez, T.J. Schmidt, ACS Catal. 2 (2012) 864–890.
[18] P. Malacrida, M. Escudero-Escribano, A. Verdaguer-Casadevall, I.E.L. Stephens, I. Chorkendorff, J. Mater. Chem. A 2 (2014) 4234–4243.
[19] A.S. Aricò, S. Siracusano, N. Briguglio, V. Baglio, A. Blasi, V. Antonucci, J. Appl. Electrochem. 43 (2013) 107–118.
[20] T. Reier, I. Weidinger, P. Hildebrandt, R. Kraehnert, P. Strasser, ECS Trans. 58 (2013) 39–51.
[21] T. Reier, M. Oezaslan, P. Strasser, ACS Catal. 2 (2012) 1765–1772.
[22] E. Antolini, ACS Catal. 4 (2014) 1426–1440.
[23] Y.J. Wang, D.P. Wilkinson, J. Zhang, Chem. Rev. 111 (2011) 7625–7651.
[24] A. Zana, J. Speder, N.E.A. Reeler, T. Vosch, M. Arenz, Electrochim. Acta 114 (2013) 455–461.
[25] L.S. Morales, A.M. Fernández, Int. J. Electrochem. Sci. 8 (2013) 12692–12706.
[26] F.-D. Kong, S. Zhang, G.-P. Yin, N. Zhang, Z.-B. Wang, C.-Y. Du, J. Power Sources 210 (2012) 321–326.
[27] J.C. Cruz, V. Baglio, S. Siracusano, R. Ornelas, L.G. Arriaga, V. Antonucci, A.S. Aricò, Int. J. Hydrogen Energy 37 (2012) 5508–5517.
[28] G. Li, H. Yu, W. Song, X. Wang, Y. Li, Z. Shao, B. Yi, Int. J. Hydrogen Energy 37 (2012) 16786–16794.
[29] T. Reier, D. Teschner, T. Lunkenbein, A. Bergmann, S. Selve, R. Kraehnert, R. Schlögl, P. Strasser, J. Electrochem. Soc. 161 (2014) F876–F882.
[30] S. Sui, L. Ma, Y. Zhai, J. Power Sources 196 (2011) 5416–5422.
[31] G. García, M. Roca-Ayats, A. Lillo, J.L. Galante, M.A. Peña, M.V. Martínez-Huerta, Catal. Today 210 (2013) 67–74.
[32] M. Roca-Ayats, G. García, J.L. Galante, M.A. Peña, M.V. Martínez-Huerta, Int. J. Hydrogen Energy 39 (2014) 5477–5484.
[33] Y. Liu, T.G. Kelly, J.G. Chen, W.E. Mustain, ACS Catal. 3 (2013) 1184–1194.
[34] C. Bock, C. Paquet, M. Couillard, G.A. Botton, B.R. MacDougall, J. Am. Chem. Soc. 126 (2004) 8028–8037.
[35] O. Guillén-Villafuerte, G. García, J.L. Rodríguez, E. Pastor, R. Guil-López, E. Nieto, J.L.G. Fierro, Int. J. Hydrogen Energy 38 (2013) 7811–7821.
[36] M. Roca-Ayats, G. Garcia, M.A. Pena, M.V. Martinez-Huerta, J. Mater. Chem. A 2 (2014) 18786–18790.
[37] R.D. Cowling, H.E. Hintermann, J. Electrochem. Soc. 117 (1970) 1447–1449.

[38] F.J. Perez-Alonso, D.N. McCarthy, A. Nierhoff, P. Hernandez-Fernandez, C. Strebel, I.E.L. Stephens, J.H. Nielsen, I. Chorkendorff, Angew. Chem. Int. Ed. 51 (2012) 4641–4643.
[39] J.C. Cruz, V. Baglio, S. Siracusano, V. Antonucci, A.S. Aricò, R. Ornelas, L. Ortiz-Frade, G. Osorio-Monreal, S.M. Durón-Torres, L.G. Arriaga, Int. J. Electrochem. Sci. 6 (2011) 6620–6627.
[40] L.-Å. Näslund, C.M. Sánchez-Sánchez, Á.S. Ingason, J. Bäckström, E. Herrero, J. Rosen, S. Holmin, J. Phys. Chem. C 117 (2013) 6126–6135.
[41] S. Cherevko, A.R. Zeradjanin, A.A. Topalov, N. Kulyk, I. Katsounaros, K.J.J. Mayrhofer, ChemCatChem 6 (2014) 2219–2223.
[42] S.M. Hoseinieh, F. Ashrafizadeh, M.H. Maddahi, J. Electrochem. Soc. 157 (2010) E50–E56.